# Dumbbell-Like Silica Coated Gold Nanorods and

# their Plasmonic Properties

- 3 Maggie Wang, Alexandra Hoff, Joseph E. Doebler, Steven R. Emory, Ying Bao\*
- 4 Department of Chemistry, Western Washington University, 98225, Bellingham, WA
  - Silica coated gold nanorods with dumbbell-like morphology allowing dual functionalization in an individual nanostructure have attracted great attention for applications such as sensing and biological imaging. We report a detailed study on the feasibility of controlling the morphology of silica coating on gold nanorods. The morphology of the silica shell can be either cylindrical or dumbbell shaped. The morphology of the silica shell can be either cylindrical or dumbbell shaped. With constant GNR concentration, the ratio of CTAB and TEOS concentration is the key to determine the amount of available TEOS for silica deposition on GNR since the TEOS will diffuse towards the surface of GNRs. The effect of morphologies on surface-enhanced Raman scattering (SERS) performance was also investigated and we found that the dumbbell morphology of silica coated gold nanorods has the most significant SERS enhancement. Our study is significant in terms of the capability to control the dumbbell morphology of silica coated gold nanorods, which can eventually broaden the application of these plasmonic nanomaterials.

## 1. Introduction

Core/shell nanostructures, one popular type of composite nanoparticles, where the core component is fully encapsulated by another component as a shell, has been widely synthesized and investigated for various applications in the areas of sensing, lelectronics, and catalysis. 3-5. Although this nanostructure provides special advantages such as maximizing the active interface between the two components, protecting the core component from surrounding environment, the core-shell structure can result in diminished direct interaction between the core material and the surrounding environment, thus, it limits uses in applications that require such direct interaction. By tuning the interface between the two components, dumbbell-like nanostructures with a partially coating covering the core can be synthesized. The coatings are separated spatially in well-defined manner, allowing both components to interact with the surrounding environment. For example, Lal and co-workers fabricated a dumbbell-like structure composed of polystyrene and silica and used it as a template for preparing silica nano-bowls.<sup>6</sup> Minko and co-workers applied biodegradable dumbbell-structured nanoparticles for local pulmonary delivery of hydrophilic and hydrophobic molecules to the lungs.<sup>7</sup> Glaser and co-workers demonstrated that dumbbell-structured nanoparticles composed of gold and iron oxide can reduce the interfacial tension at the oil/water interface significantly.8 Overall, dumbbell-like nanostructures can be useful for a variety of applications which require the core to have direct contact with the surrounding environment while still permitting the shell to provide additional functionality. Gold nanorods (GNRs) have been coupled with various coating materials to form dumbbelllike structures. When compared to spherical gold nanoparticles, an outstanding advantage of GNRs is their anisotropic structure which possesses two characteristic plasmon bands: a transverse band in the visible region and a longitudinal band in the near infrared (NIR) region.<sup>9</sup>, The longitudinal band is highly sensitive to the aspect ratio of the GNR and its environment,

1

2

3

4

5

6

7

8

9

10

11

12

13

14

15

16

17

18

19

20

21

22

1 which has lead GNRs to become one of the most popular candidates for applications in sensing<sup>11</sup>, 2 catalysis<sup>12</sup> and thermal therapy.<sup>13</sup> Researchers have fabricated GNRs with a variety of coating materials in dumbbell-like 3 morphology. 14-18 For example, Wu and co-workers coated TiO<sub>2</sub> on the tips of GNRs to form 4 5 dumbbell structures and studied their performance on photocatalytic applications. They found 6 that with this dumbbell structure, TiO<sub>2</sub> on the tips of GNRs acts as a filter for hot electrons from 7 GNRs, which satisfies the electron refilling requirement. The dumbbell structure exhibits plasmon-enhanced hydrogen evolution under visible and NIR light irradiation.<sup>18</sup> Due to the 8 9 dumbbell structure composed by the metal and semiconductor, the GNRs are partially exposed to 10 the environment, and can generate a concentrated electromagnetic field, resulting in enhanced 11 hot-electron generation and photocatalytic activity. Grzelczak and co-workers synthesized 12 dumbbell-like Au/Pt nanorods and found that Pt coated at the ends of GNRs significantly 13 enhanced absorption of light, thus producing band broadening due to the relative changes in the 14 aspect ratio after tip-coating. Such a strong shift does not occur for fully coated Pt on GNRs. 15 Such dumbbell-like Pt-coated GNRs have potential applications in which a broad spectral region is required, such as biosensing.<sup>17</sup> Overall, dumbbell morphology has been used to improve 16 17 applications in which the GNR core needs to be partially exposed to the environment. 18 Silica shells have been successfully deposited on a variety of colloidal particles of metals, metal oxides, and semiconductors. Silica coated gold nanorods (GNRs@SiO2) have several 19 20 unique properties such as high stability, adjustable morphology and shell thickness, 21 biocompatibility, and capability of surface functionalization. <sup>19</sup> GNRs@SiO<sub>2</sub> with dumbbell-like 22 morphology have been utilized for various applications. For example, Wang and co-workers

employed GNRs@SiO<sub>2</sub> as a hard template to further fabricate complex materials.<sup>20, 21</sup>

1 Szychowski and co-workers used dumbbell-like GNRs@SiO<sub>2</sub> for selectively etching GNRs with cysteamine, resulting in elongated and sharpened tips for the GNRs.<sup>22</sup> While those studies have 2 3 used GNRs@SiO<sub>2</sub> with dumbbell morphology for various purposes, they have not investigated 4 the ability to control attributes of this morphology, including the shell thickness and the shell 5 material distribution over the GNRs, which are important for fine-control of the LSPR property 6 and will eventually impact the use of GNRs. 7 This paper describes our detailed study on the controllability of dumbbell morphology of 8 silica-coated GNRs. By varying chemical concentrations in the syntheses, the morphology of 9 GNRs@SiO<sub>2</sub> can be tuned between dumbbell and cylinder. Of these two, the dumbbell 10 morphology shows a less than 17 nm red shift of the longitudinal plasmon band, which is smaller 11 shift than the shift with cylindrical morphology (more than 25 nm), indicating a smaller impact 12 to LSPR properties. Additionally, the silica shell thickness can be controlled, which further 13 impacts LSPR properties. Finally, the impacts of both morphologies on the surface-enhanced resonance Raman scattering (SERS) performance are investigated with the dumbbell 14 15 morphology having better performance.

## 2. Experimental Section

17 2.1 Materials.

16

18 Hexadecyltrimethylammonium bromide trihydrate (CTAB), gold (III)chloride 19 (HAuCl<sub>4</sub>·3H<sub>2</sub>O), L-ascorbic acid (L-AA), hydrochloric acid (HCl), tetraethylorthosilicate (TEOS), ammonium hydroxide (NH<sub>4</sub>OH), and ethanol (EtOH) were purchased from Sigma-20 21 Aldrich (USA). Sodium borohydride (NaBH<sub>4</sub>) was purchased from Merck, and silver nitrate (AgNO<sub>3</sub>) was purchased from Fisher Scientific (USA). All chemicals were used as received 22 23 without further purification.

- 1 2.2 Synthesis of Gold Nanorods.
- Gold nanorods were synthesized via a seed-mediated growth method.<sup>23</sup> To prepare the seeds,
- 3 0.250 mL of 0.01 M HAuCl<sub>4</sub> was added to 10.0 mL of 0.1 M CTAB. 0.600 mL of 0.01 M
- 4 NaBH<sub>4</sub> was then added. The solution color changed from orange to light brown, indicating the
- 5 formation of gold seeds. The solution was stirred for 2 min and left to stand for 2 hrs. For the
- 6 growth solution, a solution of surfactants was first prepared by dissolving 1.445 g of CTAB into
- 7 40 mL nanopure water at 45 °C and cool to room temperature before use. Then, 2.0 mL of 0.01
- 8 M HAuCl<sub>4</sub> and 0.800 mL of 1 M HCl were added to the surfactant solution and shaken for 30
- 9 seconds. This was followed by the addition of 0.400 mL of 0.01 M AgNO<sub>3</sub> and 0.320 mL of 0.1
- 10 M L-AA and shaken for another 30 seconds. Finally, 0.096 mL of Au seed solution was added
- and the solution was shaken for 30 seconds and then left in a 35 °C water bath for at least 16 hrs.
- 12 The final products were isolated and collected by centrifugation at 18,000 rpm for 15 min and
- were dispersed in 40 mL nanopure water.
- 14 2.3 Example of Synthesis of Silica Coating for GNRs
- 15 The method reported by Nikoobakht was employed for the silica coating of GNRs.<sup>24</sup> In a
- typical synthetic process, after the initial synthesis and purification, 15.0 mL of gold nanorod
- solution was centrifuged a second time at 18,000 rpm for 15 min. The supernatant was removed
- and the precipitate was dispersed into 10.0 mL of 1 mM CTAB solution. During gentle stirring,
- 19 0.1 M NH<sub>4</sub>OH was added to adjust the pH to 10.4. Then, three 5 μL injections of 20% (v/v)
- TEOS in ethanol was added to the solution at 30 min intervals. The solution was then left under
- stirring conditions for at least 12 hrs at room temperature. Then, the solution was centrifuged and
- 22 washed with ethanol two times at 12,500 rpm for 8 min. After that, the sample was ready for
- 23 characterization.

- While this basic approach to synthesizing silica coating will be used throughout the paper, we
- 2 have made some modifications in order to study the structural control of GNRs@SiO<sub>2</sub>.
- 3 Modifications were done on CTAB concentrations, volume percentage of TEOS in ethanol, and
- 4 amount of TEOS. The specifics of how the quantities of these three chemicals are changed from
- 5 this example approach will be discussed later.
- 6 2.4 Material Characterization.
- 7 Scanning transmission electron microscopy (STEM) imaging was conducted using a JOEL-
- 8 7200F field emission SEM operated at 30 kV. All the material sizes were measured via STEM
- 9 images by ImageJ software. The STEM samples were prepared by drop casting samples onto
- 10 copper grids. UV-vis absorption spectra were measured using a Jasco V 670 UV-Vis-NIR
- 11 spectrophotometer. The SERS spectra were acquired on a Raman spectrometer (DeltaNu
- Advantage 633) equipped with a laser (632.8 nm) with an intensity of approximately 3 mW at
- 13 the sample surface. Samples were prepared by adding 5 μL of crystal violet (100 μM) solution
- 14 into 1 mL of silica-coated gold nanorods. The solution was mixed homogenously and left
- 15 undisturbed overnight. Then, the solution was centrifuged to remove excess CV and dispersed in
- ethanol or water solvent, ready for characterization. All Raman spectra of silica coated GNR
- samples were obtained at ethanol solvent; the Raman spectrum of CTAB coated GNRs were
- 18 obtained in water solvent. The focal length is 16.45 mm. The integration time for all spectra is
- 19 10 s except when special noted.

#### 3. Results and Discussion

- 21 The overall coating process to obtain nanorods with the dumbbell morphology is schematically
- shown in Figure 1a. The successful formation of dumbbell-like nanostructures is based on a
- 23 careful control of chemical concentration and pH value. As discussed in the experimental

section, the GNRs were prepared via the seed-mediated approach. After purification, the GNRs were stabilized with extra CTAB in aqueous solution. The silica encapsulated GNRs were prepared by injecting shell precursor solution (TEOS) three times into the GNR solution. The coating process was performed in a water/ethanol cosolvent condition. The morphology of as-synthesized GNRs and dumbbell GNRs@silica were characterized with scanning transmission electron microscopy (STEM). The We observed that the as-synthesized GNRs possessed a uniform and well-defined rod-like structure with an average length and aspect ratio of 53 nm  $\pm 10$  nm and  $3.9 \pm 0.8$ , respectively, as seen in Figure 1b. The yield of synthesized GNRs is about ~95 %, obtained from STEM images with low magnification. A careful silica 

GNRs is about ~95 %, obtained from STEM images with low magnification. A careful silica coating based on receipt mentioned above can result in silica deposited at both ends of the gold nanorods (Figure 1c). Compared to gold, silica is more transparent under the scanning transmission electron microscope because the darkness of STEM depends on the atomic number of the material in the sample. Material with a lower atomic number (here, silica) are more easily penetrated by the electrons and will be more transparent in the image than material with larger atomic numbers (here, gold). The thickness of the silica shell on the end of gold nanorods in

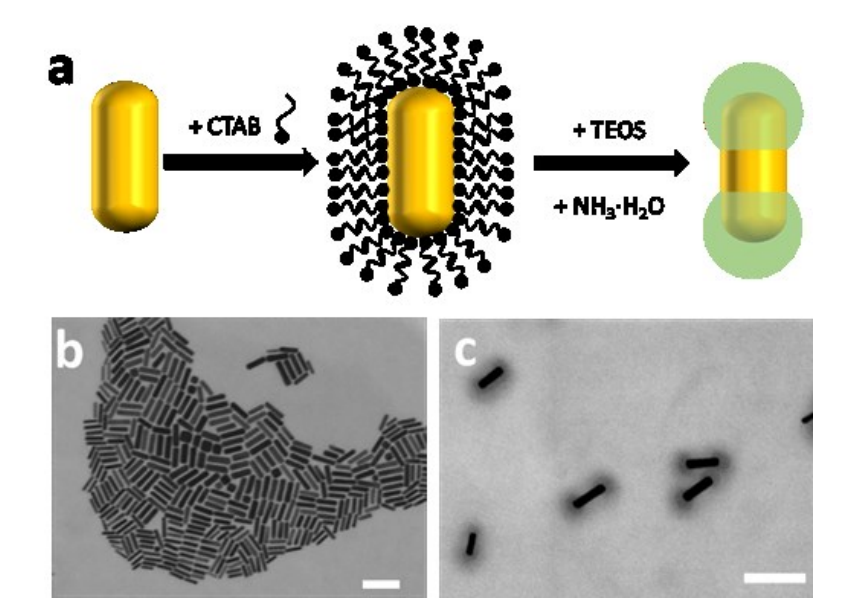


Figure 1. a) Schematic illustration for the preparation of dumbbell morphology of GNRs@SiO<sub>2</sub>;
 b) STEM image of the as-synthesized GNRs; c) STEM image of the as-prepared dumbbell
 morphology of GNRs@SiO<sub>2</sub>. Synthetic conditions: 1 mM CTAB, 15 μl of 20% (v/v) TEOS in
 ethanol, pH ≈ 10.4. Scale bar: 100 nm.

Controlling the location of silica deposits. The morphology of silica materials is highly

dependent on the experimental conditions during the silica coating. Concentration changes in chemicals such as CTAB, ethanol, and TEOS may significantly alter the size and shape of silica by affecting the nucleation and growth.

The CTAB molecule serves as a template for the deposition of silica, and its concentration will affect silica morphology. Our results showed that CTAB concentration is an important factor for determining the location of silica deposition. In this study, in order to control CTAB concentration, GNRs were centrifuged twice after synthesis, so the concentration of CTAB was less than 0.01 mM.<sup>25</sup> Then, we re-disperse purified GNRs back into solutions with various concentrations of CTAB before the process of silica coating. In all cases, we used 6 μL TEOS

1 (30 μL of 20% TEOS in ethanol). The impact of CTAB concentration on silica coating is shown 2 in Figure 2 a-c. 3 When the purified GNRs were re-dispersed into a solution with 1 mM CTAB, we found that 4 individual GNRs were still separated from each other after the silica coating, and GNRs were 5 fully encapsulated by silica. Under such conditions, the resulting diameters of the silica-coated 6 GNRs are very similar at the middle of GNR (r1, in Figure 2) as at the end (r2, in Figure 2), 7 which indicates that in this case, the silica's morphology on GNRs is cylindrical (r1/r2 close to 8 1). The cylindrical morphology of GNRs@SiO<sub>2</sub> remains for samples synthesized with 2, 3, 4 or 9 5 mM CTAB (Figure S1a-d) solutions. However, by further increasing the CTAB concentration 10 to 6, 7, 8 and 9 mM, we find that the silica shell becomes non-uniform. Some GNRs have a 11 thinner silica shell in the center than at the end, resulting in a dumbbell morphology with the 12 r1/r2 ratio being less than one (Figure 2c). These relationships between the CTAB concentration 13 and the r1 and r2 values are summarized and plotted in Figure 2c. It clearly shows that with a higher concentration of CTAB, the diameter at the ends of the GNRs (r2) remains largely 14 15 unchanged, and the diameter in the middle of the GNR (r1) falls substantially. This implies the 16 morphology evolves from cylindrical to dumbbell as the CTAB concentration increases. When 17 the CTAB concentration reaches up to 9 mM, the r1/r2 width ratio is below 1 and has a small 18 standard deviation (0.55  $\pm$  0.17) which means that most of the silica coating has a dumbbell 19 morphology as seen in Figure 2b. 20 When the concentration of CTAB is at 6 mM, the observed r1/r2 ratios have a larger standard 21 deviation than at other observed concentrations (0.72  $\pm$  0.28), and those observed ratios both 22 include approximately one as well as substantially less than one (Figure 2c). This indicates that

at this level of CTAB concentrations, there is a mixture of both cylinder and dumbbell morphologies of silica coating (Figure S1e).

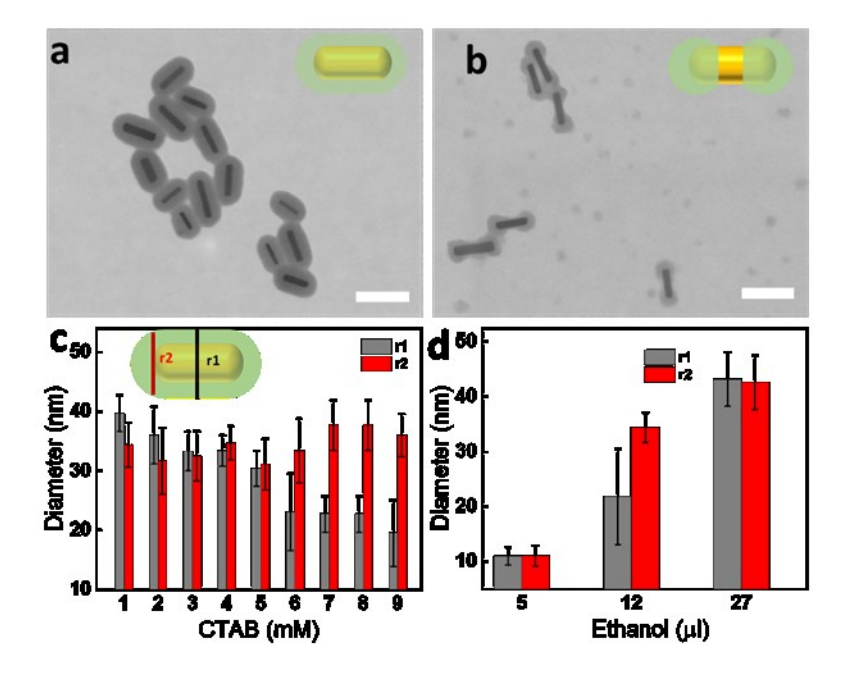


**Figure 2.** (a-b) STEM images of GNRs@silica with increasing CTAB concentrations. a) 1 mM b) 9mM; insets are corresponding model for morphology of GNRs@SiO<sub>2</sub>; c) the diameter at the center of GNRs@SiO<sub>2</sub> (r1) and at the end GNRs@SiO<sub>2</sub> (r2) as a function of additional CTAB concertation. d) the diameter from center (r1) and the end (r2) of GNRs@SiO<sub>2</sub> as a function of ethanol amount. Scale bar: 100 nm.

Another key factor for controlling the location of silica deposition is the amount of ethanol mixed with the TEOS. Ethanol is used to improve the solubility of hydrophobic TEOS in solvent, and more importantly, it changes the CTAB distribution around GNRs to facilitate TEOS diffusion to the surface of GNRs.<sup>26</sup> Figure 2d summarizes how the diameters of the silica shell change with the amount of ethanol. When the TEOS was used with only 5 µL ethanol as shown in Figure S2a, barely any silica appears on the surface of the GNRs. This indicates that with little ethanol, it is difficult for TEOS to be hydrolyzed for silica coating on the surface of

- 1 GNRs, as the TEOS is hydrophobic. When TEOS is mixed with additional ethanol using a
- 2 volume ratio of about 1:4 (ethanol is 12 μL), TEOS started depositing silica at the end of GNRs,
- 3 forming the dumbbell structure (shown in Figure S2b, identical to Figure 3c. When a TEOS-to-
- 4 ethanol volume ratio of 1:9 (ethanol is 27 μL) was used, the silica fully encapsulates the GNRs
- 5 with a uniform coating as shown in Figure S2c, creating the cylindrical morphology.
- 6 Controlling the thickness of silica deposits. The amount of TEOS used as silica precursor is
- 7 another critical factor for controlling the silica deposition on GNRs. In Figure 1c, 3 μL TEOS
- 8 (15 μL 20% TEOS in ethanol, 1mM of additional CTAB solution) was used and silica was
- 9 primarily deposited on the ends of GNRs due to the relatively low amounts of TEOS, resulting in
- the dumbbell morphology.
- When increasing the amount of TEOS and ethanol mixture (the volume percentage of TEOS in
- 12 ethanol is maintained at the same level), the additional TEOS will attach near the center of
- 13 GNRs. For example, when using 4.2 µL TEOS (Figure 3a), the surface of GNRs@silica is now
- 14 fully encapsulated by silica, though it remains thicker near the ends than at the center. As the
- amount of TEOS increases to 6  $\mu$ L, the thickness of silica continues to increase.
- The overall relationship between the TEOS amount and the average silica shell thickness at the
- 17 center of the GNRs can be found in Figure 3c. When increasing the TEOS volume from 3  $\mu$ L to 6
- 18 μL, the average thickness of the silica shell at the midpoint of the GNRs gradually increases from
- 19  $13.2 \pm 2.2$  nm to  $19.8 \pm 2.5$  nm, and the morphology of silica shell switches from dumbbell to
- 20 cylindrical. It is notable that using additional TEOS beyond 6 μL did not result in a thicker silica
- shell. This is because the reaction time between each addition of TEOS is fixed at 30 minutes so
- 22 when relatively large amounts of TEOS are used, it does not have enough time to fully condense
- 23 to silica. A control experiment has been conducted where we add TEOS with 5 min interval,

- here the silica shell thickness was  $15.2 \pm 2.1$  nm instead of  $19.8 \pm 2.5$  nm as was obtained with a
- 2 30 min interval. The STEM is shown in Figure S3. Similar results have been reported by
- 3 others.<sup>27</sup>

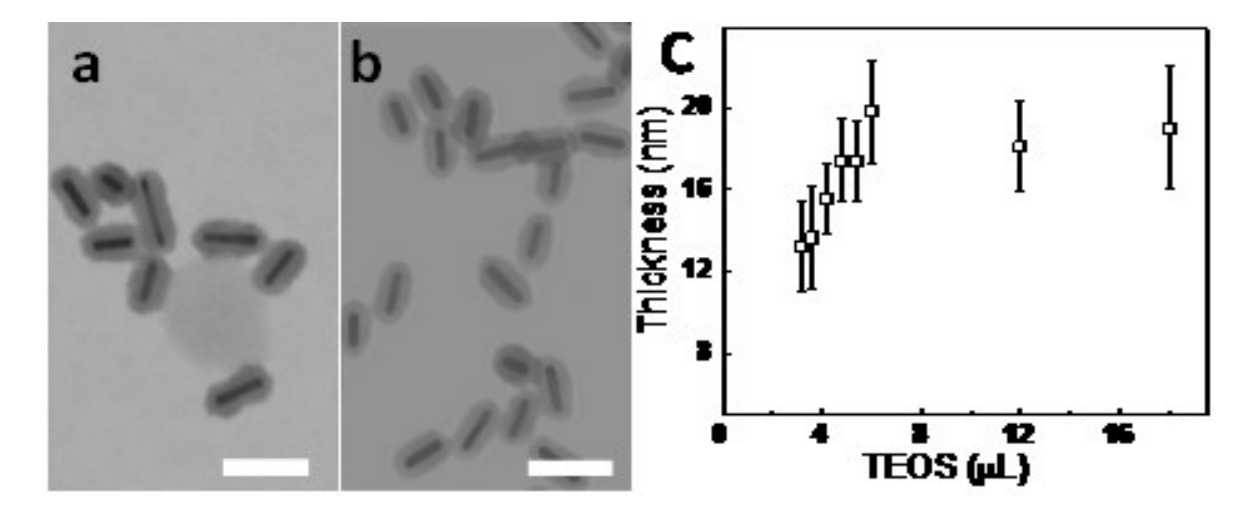


**Figure 3.** (a-b) STEM images of GNRs@SiO<sub>2</sub> with increased amount of TEOS (20% v/v in ethanol); a) 4.2 μL; b) 6 μL c) silica shell average thickness at center of GNR as a function of increased amount of TEOS. Scale bar: 100 nm.

Mechanism. In our colloidal solutions, GNRs are surrounded by a double layer of CTAB of varying densities, which dynamically exchange one layer of CTAB with free CTAB in the bulk solution. <sup>28</sup> In addition to stabilizing GNRs as surfactants, the CTAB acts as a template on GNRs for the TEOS. TEOS is the precursor of silica which prefers to interact with the hydrophobic ends of CTAB -- located in the middle of the CTAB double layer -- and then condenses to silica. In our study, the preference for deposition location for TEOS –and thus the ultimate location of the silica deposits – is highly dependent on the chemical situation of the GNRs' surface, as well as on the potential presence of CTAB micelles in the solution which were composed of excess CTAB.

Essentially, as the CTAB concentration increases, the ability of CTAB double layer to retain TEOS grows, but the strength of energy barrier that the TEOS needs to cross to get inside the double layer grows as well. This strengthening occurs at different rates on different areas of the GNR, with the sides of the GNRs having stronger energy barriers than the ends. Silica deposition will ultimately be found where there is a sufficiently strong double-layer of CTAB to keep the TEOS in place when there is enough TEOS so it can cross the energy barrier. Increasing the TEOS concentration allows the TEOS to surmount stronger CTAB energy barriers.

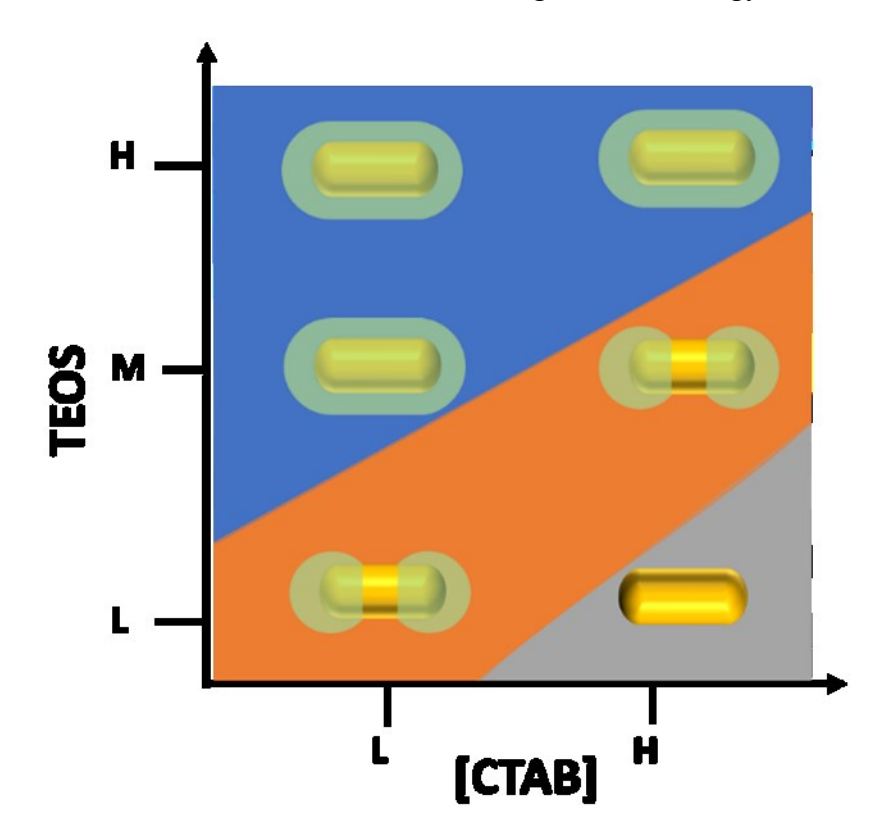


Figure 4. The morphology formations of GNRs@SiO2 under various conditions.

Figure 4 summarizes how changing levels of CTAB and TEOS impact the morphology of the silica coating. This figure includes three colored regions corresponding to no coating, dumbbell morphology and cylindrical morphology.

The grey area in Figure 4 is where no silica is coated on the GNR's surface. In this area, the ratio of TEOS to CTAB is small and the TEOS is not able to overcome the CTAB energy barrier and be adsorbed in the middle of the CTAB bilayer. Thus, no coating will occur. This area corresponds to results from Figure S5b. By increasing the ratio of TEOS to CTAB, the silica formed on the GNR's surface with a dumbbell morphology, shown in the orange area. This is because the bilayer of CTAB is less ordered and less dense at the end of GNRs than on the side owing to the larger curvature at the end. It would thus take more energy for TEOS to penetrate and condense on the side of GNRs than at the end. When the amount of TEOS available to GNRs is relatively low, TEOS will be unable to surmount the energy barrier on the sides of the silica and will instead only penetrate the CTAB at the ends of the GNRs where the energy barrier is lower, resulting in silica the deposition of silica at these locations. This area corresponds to results from Figures 1c and 2b. The blue region is where the cylinder morphology of silica coating is formed. Here, the ratio of TEOS to CTAB is very high. The TEOS will be able to overcome the higher CTAB energy barrier on the sides of the GNRs, as well as at the ends. In this case the TEOS can fully penetrate the double layer of CTAB and condense to silica around the GNRs. This area corresponds to results from Figures 3a-b, S4d and S5a. An alternative way to have the TEOS penetrate this energy barrier is to increase the amount of ethanol in the solution. When additional ethanol is present in the solution, the CTAB distribution on the surface of GNRs is changed due to the reduced polarity of solution. The density of CTAB on the side of the GNRs is decreased, which allows the TEOS to more easily penetrate the CTAB layer on the GNRs. Thus, in a situation where a normal level of ethanol would result in a dumbbell morphology, increasing the amount of ethanol can result in the silica

1

2

3

4

5

6

7

8

9

10

11

12

13

14

15

16

17

18

19

20

21

22

1 fully encapsulating the GNR with uniform coating, resulting in the cylindrical morphology 2 (Figure S2c). 3 LSPR Impact. The LSPR property of dumbbell GNRs@SiO<sub>2</sub> was studied by UV-vis 4 spectroscopy. Figure 5a shows the UV-vis absorption spectra of as-synthesized GNRs without a 5 silica coating (black line) and GNRs@SiO<sub>2</sub> with the dumbbell morphology using 15 μL of 20% 6 TEOS in ethanol and 1mM CTAB (blue line). In both spectra, two distinct peaks can be 7 observed at around 515 nm and 800 nm which are assigned to the transverse and longitudinal plasmon resonances, respectively. 21, 29, 30 Comparing the two spectra, we found that they have a 8 9 similar extinction peak at 515 nm (transverse peak), while the longitudinal peak shifted from 800 10 nm to 809 nm after the silica coating. It is known that the longitudinal peak is extremely sensitive to the dielectric constant of the immediate environment.<sup>31</sup> Such a shift could be due to 11 12 the increase in the local refractive index of the media surrounding the GNRs. Initially, the GNRs 13 were surrounded by water (with a refractive index of 1.33). After the silica coating with 14 dumbbell morphology, parts of the GNRs were instead surrounded by silica (with a refractive 15 index of 1.46) 16 As the amount of TEOS in the reaction increased, the LSPR peak was clearly continuously red shifted (Figure 5b). The amount of TEOS results in both morphology and shell thickness 17 18 change. The increased shell thickness, meaning the thickness at the center of the GNR, will 19 cause the morphology to change from dumbbell to cylindrical, which impacts the LSPR red 20 shifting. Once the morphology reaches to cylindrical, even with more TEOS, the thickness of 21 silica shell does not vary anymore. As shown in Figure 5c, this additional red shifting continued 22 until the TEOS volume reached approximately 4.8 µL. This is because after that point, the 23 excess TEOS did not result in increased thickness of the silica shell, as seen earlier in Figure 3c.

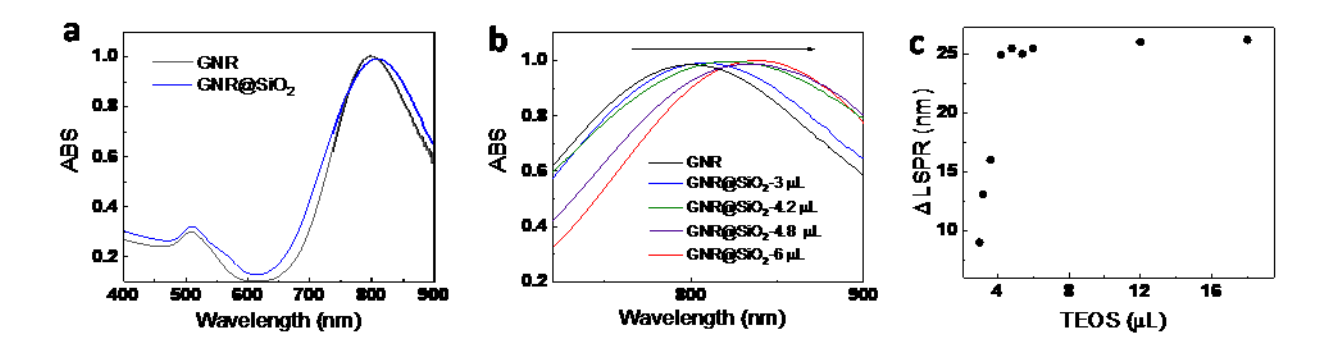


**Figure 5.** (a) UV-to-NIR spectra of GNRs before and after silica deposition forming dumbbell morphology (3  $\mu$ L TEOS); (b) NIR spectra of samples corresponding to each synthetic condition (TEOS amount: 3  $\mu$ L, 4.2  $\mu$ L, 4.8  $\mu$ L and 6  $\mu$ L); c) The variation of LSPR peak of samples with different amount of TEOS;

SERS Performance. It has been known that GNRs can be used as effective SERS substrates due to their superior SERS enhancement compared to gold nanospheres<sup>32</sup>. We examined how the dumbbell morphology for GNRs@SiO<sub>2</sub> affects the SERS enhancement for molecular sensing applications as compared to other morphologies. Crystal violet (CV) was used as a probe molecule to evaluate the SERS enhancement of the dumbbell GNRs@SiO<sub>2</sub>.

Figure 6a shows a SERS spectrum of CV adsorbed on the dumbbell GNRs@SiO<sub>2</sub> (3 μL TEOS, 12 μL ethanol, 1mM CTAB). The bands in the SERS spectrum at 912, 1173 and 1379 cm<sup>-1</sup> are assigned to the ring skeletal vibrations, C–H in-plane bending vibrations and N-phenyl stretching, respectively. The bands at 1535, 1591 and 1620 cm<sup>-1</sup> are attributed to ring C–C stretching.<sup>33</sup> As the TEOS increases over the range of 3 μL to 6 μL while maintaining other chemical amount the same, the relative SERS intensity is decreased (Figure 6b). Over this range, the average thickness of the silica shell is increasing, and the morphology is becoming more like a cylinder, as seen in Figure 3c. We hypothesize the weakened SERS is due to the increased silica shell thickness and eventual full encapsulation of silica on GNRs, leading to diminished

contact of GNRs with the surrounding environment. The effect of silica coating on SERS response was also reported by B. Bassi *et. al.*<sup>34</sup> They studied how the thickness of a thin layer of silica on the surface of gold nanostar impacts the SERS response. Similar with our finding, they found that the thin layer of silica reduces the SERS performance of gold nanostars. The SERS intensities of CV on dumbbell morphology of GNRs@SiO2 (3 µL TEOS) and bare CTAB coated GNRs were also compared shown in Figure S6. From the results, it is clear that the SERS intensity from GNRs@SiO2 with dumbbell morphology (3 µL TEOS) is about 10 times stronger than the SERS intensity from bare CTAB coated GNRs. It is also worth mentioning that the CTAB coated GNRs are unstable in ethanol solution while the GNRs@SiO2 are stable in both water and ethanol phase. Thus, the SERS experiment for CTAB coated GNRs is carried out in the water phase.

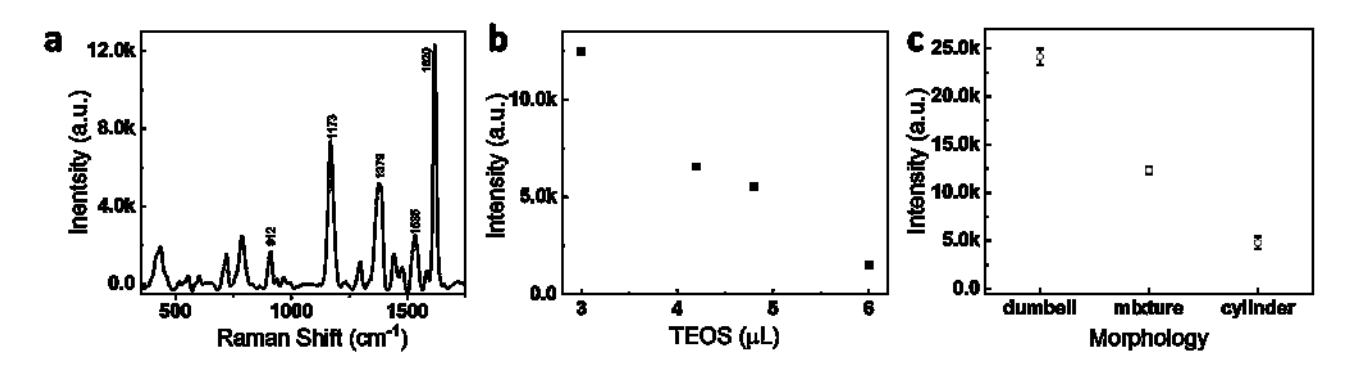


Figure 6. (a) SERS spectrum of CV on dumbbell morphology of GNRs@SiO<sub>2</sub> (3 μL TEOS); (b) SERS intensity variation of band at 1620 cm<sup>-1</sup> as a function of the amount of TEOS; (c) SERS intensity of band at 1620 cm<sup>-1</sup> comparison among various morphologies.

To find further evidence supporting this hypothesis, we evaluated the SERS performance of GNRs@SiO<sub>2</sub> for samples that were predominantly dumbbell, predominantly cylindrical, and a mixture of the two obtained from experiments discussed previously in Figures 3 and 4. In this case, the "predominantly dumbbell" sample is obtained from 9 mM CTAB conditions, 30 μL of

20% (v/v) TEOS in ethanol and 81.8% of the GNRs have the dumbbell morphology. The "mixture" samples are the ones that produced Figure 1c and the 6 mM CTAB result from Figure S1c. These samples feature 30.3% and 23.2% dumbbell morphology, respectively, with the remaining GNRs having a cylinder morphology. The "cylinder" results are the remaining samples used in Figures 2c and 3c and contain very few, if any, GNRs with dumbbell morphology. For the "predominantly dumbbell" sample, the enhancement factor (EF) is calculated based on eq 1.35

$$EF = \frac{I_{SERS}/C_{SERS}}{I_{RS}/C_{RS}}$$

where  $I_{SERS}$  is the intensity of Raman spectra of the sample with certain concentration ( $C_{SERS}$ ), and  $I_{RS}$  is the intensity of the normal Raman spectra obtained from same analyte solution with concentration ( $C_{RS}$ ). The detailed calculation of the EF is given in the Supporting Information, and both the SERS spectrum and Raman spectrum of crystal violet are shown in Figure S7. The EF for the "predominantly dumbbell" sample is about  $2.2 \times 10^2$ . We believe the very low EF might be because the SERS signal is coming from individual GNRs.

The summary of these results is shown in Figure 6c. The results agree with our prediction that GNRs@SiO2 with cylindrical morphology should give the lowest SERS intensity, and the dumbbell morphologies should show the highest intensity. It is understandable that the GNRs@SiO2 with cylindrical morphology shows the lowest SERS intensity due to their greater average silica thickness, and for a similar reason, it is understandable that the dumbbell morphology has the highest SERS intensity.

#### 4. Conclusions

In summary, we have demonstrated a detailed study on the controllability of dumbbell morphology for GNRs@SiO<sub>2</sub>. The concentration of CTAB and the amount of ethanol allow for

- 1 control over the location of silica deposition onto GNRs. The thickness of silica deposition can
- 2 be controlled by the amount of TEOS. The thickness increases with TEOS concentration until
- 3 the reaction time limits the silica growth on the GNRs. The LSPR of GNRs has a red shift after
- 4 the dumbbell-like silica coating, indicating the surrounding refractive index of GNRs has
- 5 increased. With increased thickness of the silica coating, LSPR has a stronger red-shift.
- 6 However, the increased thickness weakens the SERS enhancement. Compared to the cylinder
- 7 morphology, the dumbbell morphology of GNRs@SiO<sub>2</sub> shows significant SERS enhancement.

- 9 ASSOCIATED CONTENT
- 10 **Supporting Information**.
- 11 The following files are available free of charge.
- 12 Additional STEM images of silica coated gold nanorods under various synthetic conditions.
- 13 (PDF)
- 14 AUTHOR INFORMATION
- 15 Corresponding Author
- \*Ying.Bao@wwu.edu (Y.B.)
- 17 Notes
- 18 There are no conflicts to declare.

- 20 ACKNOWLEDGMENT
- This research was supported by Western Washington University, Department of Chemistry.
- 22 STEM studies were conducted on instrument is funded by the Joint Center for Deployment and

- 1 Research in Earth Abundant Materials (JCDREAM). The authors are grateful to all the members
- 2 in Bao group for the valuable discussion. M. W. thanks the partial support from the NSF REU
- 3 program.
- 4 REFERENCES
- 5 (1). Matsui, J.; Akamatsu, K.; Nishiguchi, S.; Miyoshi, D.; Nawafune, H.; Tamaki, K.;
- 6 Sugimoto, N., Composite of Au Nanoparticles and Molecularly Imprinted Polymer as a Sensing
- 7 Material. Anal. Chem. 2004, 76 (5), 1310-1315.
- 8 (2). Pardo-Yissar, V.; Gabai, R.; Shipway, A. N.; Bourenko, T.; Willner, I., Gold
- 9 Nanoparticle/Hydrogel Composites with Solvent-Switchable Electronic Properties. Adv. Mater.
- 10 2001, 13 (17), 1320-1323.
- 11 (3). Zhong, C. J.; Maye, M. M., Core-Shell Assembled Nanoparticles as Catalysts. Adv.
- 12 Mater. 2001, 13 (19), 1507-1511.
- 13 (4). Xu, Y.; Chen, L.; Wang, X.; Yao, W.; Zhang, Q., Recent advances in noble metal based
- 14 composite nanocatalysts: colloidal synthesis, properties, and catalytic applications. Nanoscale
- 15 2015, 7 (24), 10559-10583.
- 16 (5). Ghosh Chaudhuri, R.; Paria, S., Core/Shell Nanoparticles: Classes, Properties, Synthesis
- 17 Mechanisms, Characterization, and Applications. Chem. Rev. 2012, 112 (4), 2373-2433.
- 18 (6). Mo, A. H.; Landon, P. B.; Emerson, C. D.; Zhang, C.; Anzenberg, P.; Akkiraju, S.; Lal,
- 19 R., Synthesis of nano-bowls with a Janus template. Nanoscale 2015, 7 (2), 771-775.
- 20 (7). Garbuzenko, O. B.; Winkler, J.; Tomassone, M. S.; Minko, T., Biodegradable Janus
- 21 Nanoparticles for Local Pulmonary Delivery of Hydrophilic and Hydrophobic Molecules to the
- 22 Lungs. Langmuir 2014, 30 (43), 12941-12949.
- 23 (8). Glaser, N.; Adams, D. J.; Böker, A.; Krausch, G., Janus Particles at Liquid-Liquid
- 24 Interfaces. Langmuir 2006, 22 (12), 5227-5229.
- 25 (9). Bao, Y.; Vigderman, L.; Zubarev, E. R.; Jiang, C., Robust Multilayer Thin Films
- 26 Containing Cationic Thiol-Functionalized Gold Nanorods for Tunable Plasmonic Properties.
- 27 Langmuir 2012, 28 (1), 923-930.
- 28 (10). Scarabelli, L.; Hamon, C.; Liz-Marzán, L. M., Design and Fabrication of Plasmonic
- Nanomaterials Based on Gold Nanorod Supercrystals. Chem. Mater. 2017, 29 (1), 15-25.
- 30 (11). Wulf, V.; Knoch, F.; Speck, T.; Sönnichsen, C., Gold Nanorods as Plasmonic Sensors for
- 31 Particle Diffusion. J. Phys. Chem. Lett. 2016, 7 (23), 4951-4955.
- 32 (12). Mohanta, J.; Satapathy, S.; Si, S., Porous Silica-Coated Gold Nanorods: A Highly Active
- Catalyst for the Reduction of 4-Nitrophenol. ChemPhysChem 2016, 17 (3), 364-368.

- 1 (13). Chen, Y.; Bian, X.; Aliru, M.; Deorukhkar, A. A.; Ekpenyong, O.; Liang, S.; John, J.;
- 2 Ma, J.; Gao, X.; Schwartz, J.; Singh, P.; Ye, Y.; Krishnan, S.; Xie, H., Hypoxia-targeted gold
- annorods for cancer photothermal therapy. Oncotarget 2018, 9 (41), 26556-26571.
- 4 (14). Zheng, Z.; Tachikawa, T.; Majima, T., Plasmon-Enhanced Formic Acid Dehydrogenation
- 5 Using Anisotropic Pd-Au Nanorods Studied at the Single-Particle Level. J. Am. Chem. Soc.
- 6 2015, 137 (2), 948-957.
- 7 (15). Wei, Y.; Zhao, Z.; Yang, P., Pd-Tipped Au Nanorods for Plasmon-Enhanced
- 8 Electrocatalytic Hydrogen Evolution with Photoelectric and Photothermal Effects.
- 9 ChemElectroChem 2018, 5 (5), 778-784.
- 10 (16). Wang, H.; Gao, Y.; Liu, J.; Li, X.; Ji, M.; Zhang, E.; Cheng, X.; Xu, M.; Liu, J.;
- Hongpan, R.; Chen, W.; Fan, F.; Li, C.; Zhang, J., Efficient Plasmonic Au/CdSe Nanodumbbell
- 12 for Photoelectrochemical Hydrogen Generation beyond Visible Region. 2019.
- 13 (17). Grzelczak, M.; Pérez-Juste, J.; García de Abajo, F. J.; Liz-Marzán, L. M., Optical
- Properties of Platinum-Coated Gold Nanorods. J. Phys. Chem. C 2007, 111 (17), 6183-6188.
- 15 (18). Wu, B.; Liu, D.; Mubeen, S.; Chuong, T. T.; Moskovits, M.; Stucky, G. D., Anisotropic
- 16 Growth of TiO2 onto Gold Nanorods for Plasmon-Enhanced Hydrogen Production from Water
- 17 Reduction. J. Am. Chem. Soc. 2016, 138 (4), 1114-1117.
- 18 (19). Abadeer, N. S.; Brennan, M. R.; Wilson, W. L.; Murphy, C. J., Distance and Plasmon
- 19 Wavelength Dependent Fluorescence of Molecules Bound to Silica-Coated Gold Nanorods. ACS
- 20 Nano 2014, 8 (8), 8392-8406.
- 21 (20). Wang, F.; Cheng, S.; Bao, Z. H.; Wang, J. F., Anisotropic Overgrowth of Metal
- Heterostructures Induced by a Site-Selective Silica Coating. Angew. Chem. 2013, 52 (39),
- 23 10344-10348.
- 24 (21). Orendorff, C. J.; Gearheart, L.; Jana, N. R.; Murphy, C. J., Aspect ratio dependence on
- surface enhanced Raman scattering using silver and gold nanorod substrates. Phys. Chem. Chem.
- 26 Phys. 2006, 8 (1), 165-170.
- 27 (22). Szychowski, B.; Leng, H.; Pelton, M.; Daniel, M.-C., Controlled etching and tapering of
- 28 Au nanorods using cysteamine. Nanoscale 2018, 10 (35), 16830-16838.
- 29 (23). Gole, A.; Murphy, C. J., Seed-Mediated Synthesis of Gold Nanorods: Role of the Size
- and Nature of the Seed. Chem. Mater. 2004, 16 (19), 3633-3640.
- 31 (24). Gorelikov, I.; Matsuura, N., Single-Step Coating of Mesoporous Silica on Cetyltrimethyl
- 32 Ammonium Bromide-Capped Nanoparticles. Nano Lett. 2008, 8 (1), 369-373.
- 33 (25). Huang, J.; Park, J.; Wang, W.; Murphy, C. J.; Cahill, D. G., Ultrafast Thermal Analysis
- of Surface Functionalized Gold Nanorods in Aqueous Solution. ACS Nano 2013, 7 (1), 589-597.
- 35 (26). Shah, K. W.; Sreethawong, T.; Liu, S.-H.; Zhang, S.-Y.; Tan, L. S.; Han, M.-Y., Aqueous
- route to facile, efficient and functional silica coating of metal nanoparticles at room temperature.
- 37 Nanoscale 2014, 6 (19), 11273-11281.

- 1 (27). Wu, W. C.; Tracy, J. B., Large-Scale Silica Overcoating of Gold Nanorods with Tunable
- 2 Shell Thicknesses. Chem. Mater. 2015, 27 (8), 2888-2894.
- 3 (28). El Khoury, J. M.; Zhou, X.; Qu, L.; Dai, L.; Urbas, A.; Li, Q., Organo-soluble
- 4 photoresponsive azothiol monolayer-protected gold nanorods. Chem. Commun. 2009, (16),
- 5 2109-2111.
- 6 (29). Orendorff, C. J.; Gole, A.; Sau, T. K.; Murphy, C. J., Surface-Enhanced Raman
- 7 Spectroscopy of Self-Assembled Monolayers: Sandwich Architecture and Nanoparticle Shape
- 8 Dependence. Anal. Chem. 2005, 77 (10), 3261-3266.
- 9 (30). Nikoobakht, B.; Wang, J.; El-Sayed, M. A., Surface-enhanced Raman scattering of
- molecules adsorbed on gold nanorods: off-surface plasmon resonance condition. Chem. Phys.
- 11 Lett. 2002, 366 (1), 17-23.
- 12 (31). Wang, Y.; Wang, Y. Q.; Wang, W. H.; Sun, K. X.; Chen, L. X., Reporter-Embedded
- 13 SERS Tags from Gold Nanorod Seeds: Selective Immobilization of Reporter Molecules at the
- 14 Tip of Nanorods. ACS Appl. Mater. Interfaces 2016, 8 (41), 28105-28115.
- 15 (32). Lin, K.-Q.; Yi, J.; Hu, S.; Liu, B.-J.; Liu, J.-Y.; Wang, X.; Ren, B., Size Effect on SERS
- of Gold Nanorods Demonstrated via Single Nanoparticle Spectroscopy. J. Phys. Chem. C 2016,
- 17 120 (37), 20806-20813.
- 18 (33). Liang, E. J.; Ye, X. L.; Kiefer, W., Surface-Enhanced Raman Spectroscopy of Crystal
- 19 Violet in the Presence of Halide and Halate Ions with Near-Infrared Wavelength Excitation. J.
- 20 Phys. Chem. A 1997, 101 (40), 7330-7335.
- 21 (34). Bassi, B.; Albini, B.; D'Agostino, A.; Dacarro, G.; Pallavicini, P.; Galinetto, P.; Taglietti,
- A., Robust, reproducible, recyclable SERS substrates: Monolayers of gold nanostars grafted on
- 23 glass and coated with a thin silica layer. Nanotechnology 2018, 30 (2), 025302.
- 24 (35). Le Ru, E. C.; Blackie, E.; Meyer, M.; Etchegoin, P. G., Surface Enhanced Raman
- 25 Scattering Enhancement Factors: A Comprehensive Study. J. Phys. Chem. C 2007, 111 (37),
- 26 13794-13803.

## 1 Table of Content

